Journal of Current Science and Technology, October-December 2025 Vol. 15 No. 4, Article 135

ISSN 2630-0656 (Online)

Cite this article: Tantipiriyakul, T., Kanjanasit, K. (2025). Chessboard-coding metasurface antennas with binary defects for anomalous radiation: Novel and continuous development. *Journal of Current Science and Technology*, *15*(4), Article 135. https://doi.org/10.59796/jcst.V15N4.2025.135

Journal of Current Science and Technology

Journal homepage: https://jcst.rsu.ac.th

Chessboard-coding Metasurface Antennas with Binary Defects for Anomalous Radiation: Novel and Continuous Development

Tanatorn Tantipiriyakul, and Komsan Kanjanasit*

College of Computing, Prince of Songkla University Phuket Campus, Phuket 83120, Thailand

*Corresponding author; E-mail: komsan.k@psu.ac.th

Received 9 April 2025; Revised 18 June 2025; Accepted 25 June 2025; Published online 20 September 2025

Abstract

This paper presents a numerical analysis of chessboard-coding metasurface antennas, focusing on the impact of binary coding defects on beamforming radiation characteristics. Chessboard-coding metasurface antennas, composed of 1-bit unit cells with binary phase distributions (0° and 180°), enable near-field wavefront control for beam steering applications. Beam tilting is achieved by introducing binary defects, which break phase continuity and affect radiation performance. This study investigates a planar antenna and examines the effects of binary defects in metasurface unit cells by analyzing reflection characteristics, impedance variations, and radiation patterns at 9 GHz. Twelve defect configurations are simulated to observe beam tilting and distortion patterns, revealing a strong dependence on defect location. The spatial distribution of defects within the metasurface lattice is categorized into inner and outer regions, according to their impact on beam characteristics. Numerical results show that binary defects can redirect beams in both azimuth and elevation. The defective cell locations in the 5 × 5 chessboard pattern reveal symmetric beam shifts in azimuth (0°, ±50°, ±110°, and ±137°) and elevation (+17.5° and +22.5°), with antenna gains ranging from 4.1 to 5.3 dBi compared to a 5.57 dBi baseline. Impedance bandwidths are observed approximately within the 8.4–9.5 GHz range. These findings offer valuable design insights for developing robust, reconfigurable metasurface antennas suited for next-generation 6G communication systems operating in the centimeter-wave band.

Keywords: *chessboard-coding metasurface; binary coding defects; beamforming radiation; phase discontinuities; metasurface antennas*

1. Introduction

The advancement of electromagnetic (EM) wave manipulation techniques has led to the emergence of metasurface antennas, which have demonstrated remarkable capabilities in beamforming, wavefront shaping, and polarization control. Unlike traditional phased-array antennas, which require complex phase-shifting networks and high-power-consuming components, metasurface antennas provide a compact, low-cost, and efficient solution for controlling the propagation of EM waves using subwavelength-scale resonant elements (Kanjanasit et al., 2023; Rahman et al., 2025).

Metasurface antennas are a subclass of engineered surfaces designed to manipulate EM waves through precisely arranged subwavelength unit cells. Unlike conventional antenna arrays, metasurface antennas control wavefront propagation through phase discontinuities introduced by the unit cells, which can be either passive or active (Zhang et al., 2017; Sheng et al., 2022; Wang et al., 2024; Vinod & Khairnar, 2024; Tantipiriyakul & Kanjanasit, 2024). By adjusting the phase response of individual unit cells, metasurface antennas enable functionalities such as beam steering, beam splitting, and polarization conversion. One of the most significant

advantages of metasurface antennas is their ability to operate with minimal energy consumption while maintaining high efficiency in wave manipulation. These characteristics have led to their integration into modern communication systems, where they provide solutions for dynamic beamforming and spatial signal control.

Among the various types of metasurfaces, digital coding metasurfaces have gained significant attention due to their ability to implement binary or multi-bit phase modulation in a straightforward and programmable manner. Coding metasurfaces are typically designed using a binary 0/1 encoding scheme. Digital metasurfaces encode unit cells with discrete phase states, typically '0' and '1' (corresponding to phase shifts of 0° and 180°), enabling real-time manipulation of the reflection and transmission properties of EM waves (Cui et al., 2016; Ma et al., 2022; Cui et al., 2020). Such metasurfaces have been widely investigated for applications in wireless communication, radar, satellite communication, and beamforming in 5G and beyond networks (Selvaraj et al., 2025). The concept of digital coding metasurfaces was first introduced as a means of simplifying the complex design process of traditional metasurfaces. Instead of relying on continuous phase-gradient distributions, digital coding metasurfaces use discrete phase shifts to achieve similar wavefront control effects (Cui et al., 2014). The coding strategy allows metasurfaces to be reconfigured easily using digital circuits, making them an attractive option for real-time adaptive applications. By arranging these binary-coded unit cells into specific patterns, various wavefront modulation effects can be achieved. This concept has been extended to space-time coding metasurfaces, which introduce temporal variations to further enhance the control of EM wave behavior (Zhang & Cui, 2021).

Chessboard-coding metasurfaces are a class of digital metasurfaces designed with alternating binary-coded unit cells, forming a checkerboard-like pattern. This arrangement allows for constructive and destructive interference effects, enabling precise beam shaping and wavefront manipulation. Such metasurfaces have been widely explored for their ability to control EM wave reflection and transmission efficiently (Galarregui et al., 2013; Xue et al., 2018; Tantipiriyakul & Kanjanasit, 2023). However, a major limitation of such designs is their inherently static beamforming nature, which lacks adaptability. Furthermore, while binary coding defects (particularly in clustered or spatially correlated forms) can significantly influence electromagnetic behavior, there is a lack of systematic analysis on how these defect patterns affect beam directionality, stability, and overall radiation performance.

2. Objective

This study aims to investigate how binary coding defects affect the beamforming performance of chessboard-coding metasurface antennas. Using full-wave simulations based on the finite element method (FEM), the research analyzes the influence of binary defects on radiation characteristics. Particular attention is given to how the spatial placement of defects within the metasurface lattice-especially between central (inner) and peripheral (outer) unit cells-impacts beam direction, gain, and main lobe stability. The study further characterizes the pattern distortion and beam tilting caused by different defect scenarios within a 5 × 5 chessboard-coded configuration. Based on these analyses, practical design guidelines are proposed for developing metasurface antennas that maintain directional performance despite coding imperfections. Finally, the feasibility of using binary defects as a passive method for beam steering is explored, with potential applications in future 6G centimeter-wave communication systems (Testolina et al., 2024).

3. Materials and Methods

This section outlines the methodology used to design, simulate, and analyze digital chessboard-coding metasurface antennas with binary defects for beam adjustment. The antenna performance is investigated through numerical analysis based on the Finite Element Method (FEM) using Ansys HFSS (Ansys Inc., 2024). The approach involves designing the metasurface unit cells based on digital coding principles and implementing the chessboard-coding pattern, incorporating binary defects for beam steering.

3.1 Theoretical Modeling

A chessboard-coding metasurface is an engineered surface designed to manipulate electromagnetic waves through a structured phase distribution. It consists of subwavelength unit cells, each capable of imparting a specific phase shift to the incident wave. In a binary coding metasurface, these phase shifts are typically out-of-phase, creating a chessboard-like arrangement where adjacent elements reflect waves with different phase responses. This structure allows precise control over the far-field scattering pattern,

enabling functionalities such as beam steering, wavefront shaping, and anomalous reflection. The fundamental equation governing the far-field scattering of the coding metasurface is given by:

$$F(\theta,\varphi) = \sum_{m=1}^{M}\sum_{n=1}^{N} \exp\left(j\varphi_{mn}\right) \times exp\left\{jk_0 sin\theta\left[D_x\left(m-\frac{1}{2}\right)cos\varphi + D_y\left(n-\frac{1}{2}\right)sin\varphi\right]\right\} \quad (1)$$

where $k_0 = \omega/c = 2\pi/\lambda$ represents the free-space wavenumber, and D_x and D_y define the unit cell dimensions along the x- and y-axes, respectively. The reflection phase response of each element, denoted as φ_{mn}, determines how the wavefront is modulated. The angles θ and φ define the observation direction in the far field, allowing for a comprehensive description of how the scattered waves propagate.

The cheeseboard coding pattern follows a controlled binary phase encoding strategy, where different subregions reflect incident waves with distinct phase shifts. This configuration allows constructive and destructive interference to modify the scattered wavefront, leading to significant control over the diffraction properties of the metasurface. Unlike traditional reflective surfaces, where waves obey the law of reflection, a coding metasurface redistributes energy into multiple diffraction orders by engineering the phase response of its elements. The exponential phase term $\exp\left(j\varphi_{mn}\right)$ in the equation represents the local phase shift introduced by each metasurface element, while the summation accounts for contributions from all unit cells. This collective behavior determines how waves interfere in the far field, resulting in beam steering, wave redirection, or diffraction pattern manipulation.

3.2 Chessboard-Coding Metasurface Antenna Structure

Figure 1 illustrates the structural design and modified configuration of a chessboard-coding metasurface antenna, highlighting different stages of the coding pattern implementation and feeding mechanism. The metasurface antenna design is presented in five subfigures, labeled (a)–(e), depicting the patch array structure, coding distribution, coordinate system, feeding mechanism, and side-view layout. This design approach is crucial because it leverages the phase response of coding elements. Based on the study by Kanjanasit et al. (2023), the planar artificial magnetic conductor (AMC) antenna was analyzed in terms of its dimensions, and a 5 × 5 metasurface configuration was recommended as optimal for high-gain enhancement. A larger patch lattice dimension can lead to radiation degradation due to non-uniform near-field interactions that disrupt phase coherence across the metasurface. Figure 1a illustrates a top view of a 5 × 5 uniform square patch array, where each patch unit cell is assigned a binary state of '1'. In this configuration, '1' represents AMC elements, which are known for their zero-degree reflection phase properties. AMC elements act as high-impedance surfaces, allowing constructive interference of reflected waves. When an incident electromagnetic wave impinges on this metasurface, the AMC elements ensure that the reflected wave remains in-phase, which is essential for wavefront shaping and beam redirection applications. This configuration serves as a baseline metasurface structure, where all elements have the same reflection characteristics, resulting in a uniform phase distribution.

Figure 1b depicts a modified chessboard-coding metasurface, where unit cells are assigned binary states '0' and '1', creating an alternating checkerboard-like structure. Here, the binary state "0" represents perfect electric conductor (PEC) elements, which introduce a 180° phase shift (out-of-phase reflection phase) in contrast to the AMC elements with zero-degree reflection phase. By alternating between AMC and PEC elements, the metasurface introduces phase discontinuities that enhance wave scattering capabilities. This structure is widely used to generate diffuse reflection, improving electromagnetic stealth and beamforming efficiency. The presence of PEC elements ensures that incident waves are scattered in multiple directions, disrupting coherent reflection. The combination of '1' and '0' states is the fundamental principle behind coding metasurfaces, enabling precise control of reflected wavefronts.

Figure 1c presents the physical coordinate system in the x-y plane, allowing the identification of each unit cell location in the metasurface. The rows are labeled "A–E" and columns as "1–5", forming a grid-like system for referencing individual unit cells. This labeling scheme is essential for analyzing localized phase responses and tuning specific unit cells with defects. The coordinate system enables systematic defect identification and phase optimization of unit cells. Certain unit cells can be selectively modified to achieve anomalous electromagnetic behaviors.

Figure 1d illustrates the bottom-layer schematic layout of the coplanar waveguide (CPW)-fed aperture feeder, which is responsible for exciting the metasurface structure. The CPW-fed aperture mechanism consists of a short-end configuration, allowing efficient coupling of electromagnetic energy into the metasurface. CPW-fed apertures offer several advantages, including wideband impedance matching, low-profile integration, and ease of fabrication. The short-end CPW aperture design enhances field coupling between the feeding and the metasurface patches, ensuring efficient wave excitation and controlled radiation characteristics. This feeder design plays a crucial role in achieving resonant behavior at the desired operating frequency, typically around 9 GHz in operation.

Figure 1e presents a side-view schematic of the two-layer metasurface antenna, illustrating the layered structure of the metasurface assembly. The metasurface consists of an upper layer with a patch array and a substrate layer made of FR4 dielectric material. The FR4 substrate provides mechanical support and ensures proper impedance matching for efficient electromagnetic wave interaction. The CPW-fed aperture is located beneath the substrate, enabling electromagnetic energy coupling to the upper metasurface layer. The layered configuration allows the metasurface to function as a resonant cavity, optimizing wave reflection and beamforming properties. This design facilitates high-gain radiation, low-profile integration, and frequency-selective response, making it suitable for applications in wireless communication using beamforming antennas.

The optimized design parameters of the proposed metasurface antenna are summarized in Table 1. According to Balanis (2005), the driven feeder consists of a narrow aperture element with a designed length (Ls) = 14 mm and width (Ws) = 1.0 mm. The length Ls is theoretically derived from one wavelength at ~9 GHz, while the Ws parameter is initially estimated as one-tenth of the aperture width during the preliminary design phase. Based on Simons (2001), the primary design of the short-ended CPW feeder, with a 50-Ω characteristic impedance, includes a feedline width (Wf) = 2.0 mm and a gap (G) = 0.2 mm, guiding the wave signal to the narrow aperture efficiently. The metasurface comprises a FR4 dielectric slab (relative permittivity ε_r = 4.4, loss tangent = 0.025), positioned between the primary feeder and a 5 × 5 chessboard-patterned patch array. The design parameters of the square patch-based chessboard pattern are derived from the supercell configuration analysis. To design the metasurface structure, a frequency selective surface (FSS) composed of square patches backed by a ground plane is employed. This configuration acts as an AMC, reflecting incident waves in-phase at its resonant frequency, as described by Feresidis et al. (2005). For an AMC, resonance occurs when the reflection phase reaches 0° at the target frequency (f_o). The patch size and unit cell period are determined using both analytical and empirical methods to achieve resonance under normal incidence. The effective wavelength in the dielectric medium is calculated as follows:

$$\lambda_{eff} = \frac{c}{f_o\sqrt{\varepsilon_{eff}}} \ , \ \varepsilon_{eff} \approx \frac{\varepsilon_r+1}{2} \qquad (2)$$

where c denotes the speed of light in free space, given as 3×10^8 m/s. The resonant patch array arrangement for the AMC is approximated to operate at 9 GHz, using $P \approx 0.2\lambda_{eff}$, where P is the unit cell periodicity. For this design, the array period (P) = 3.9 mm, and the patch length (L) = 3.7 resulting in an inter-element gap of approximately 0.2 mm. In this coding metasurface, two types of unit cells are defined: binary '1' elements, represented by a partial patch (L = 3.7 mm, P = 3.9 mm), and binary '0' elements, which are full patches (L = P = 3.9 mm). The overall planar metasurface structure has dimensions of 25 × 25 mm² (~0.75λ × ~0.75λ at 9 GHz), ensuring compatibility with the designed frequency range and enabling efficient electromagnetic wave manipulation.

Table 1 Physical dimensions of a chessboard-coding metasurface antenna comprising a patch array and a narrow CPW-fed aperture, presented in millimeters (mm)

P	L	Ls	Ws	Wf	G	H
3.9	**3.7**	14	1.0	2.0	0.2	2.4

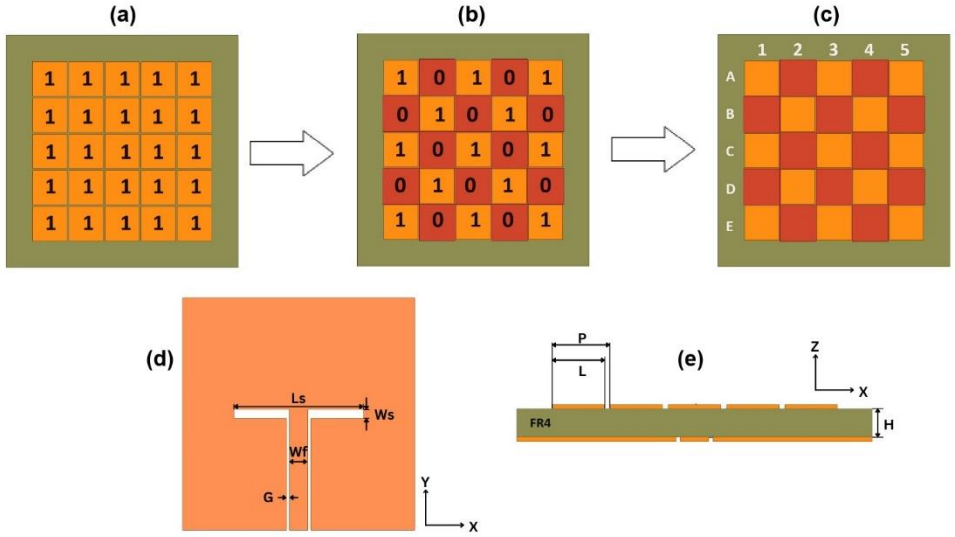

Figure 1 Structural design of the chessboard coding metasurface antenna: (a) Uniform 5×5 AMC patch array (binary '1'); (b) Alternating AMC/PEC coding (binary '1'/'0') for phase control; (c) Unit cell identification using X–Y coordinates; (d) CPW-fed aperture with short-end excitation; (e) Side view showing two-layer structure with FR4 substrate

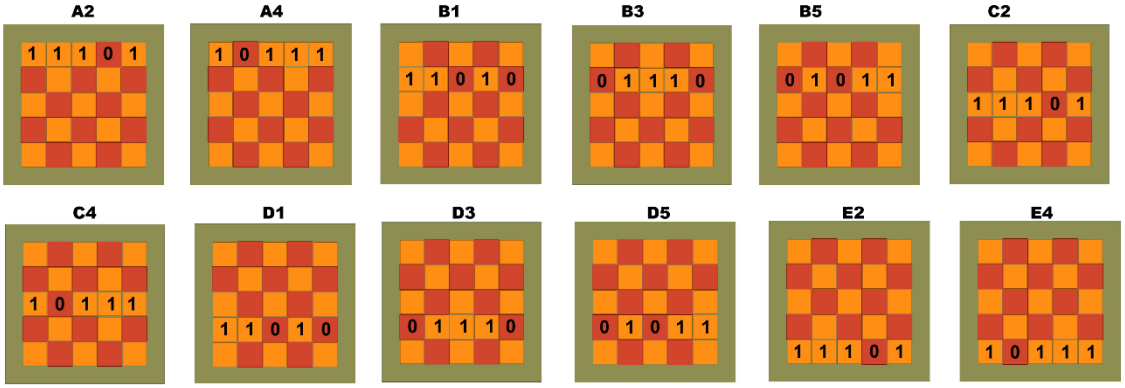

Figure 2 Illustration of twelve defective unit-cell configurations in a chessboard-coded metasurface, including cells A2, A4, B1, B3, B5, C2, C4, D1, C3, C5, E2, and E4, where the digital sequence uses '0' and '1' to represent 180° and 0° reflection phases, respectively

3.3 Binary Chessboard-Coding and Defective Implementation

In metasurfaces, binary states control phase response, and a chessboard pattern enables beam manipulation. Defects in the coding disrupt phase continuity, affecting reflection, impedance, and radiation behavior. To implement binary defects, selected individual unit cells of '0' state are systematically replaced with '1' state unit cells, introducing localized phase discontinuities within the metasurface structure. This defective strategy alters the uniform phase distribution, leading to the controlled beam radiation. By optimizing the placement of defected unit cells, the metasurface can achieve the beam forming. The binary defects process enables beam control over the reflected wavefront. Figure 2 illustrates twelve distinct unit-cell configurations with defective binary coding sequences in a chessboard-coding metasurface design. Each unit cell, labeled as A2, A4, B1, B3, B5, C2, C4, D1, C3, C5, E2, and E4, features a unique binary coding pattern composed of '0' and '1' state.

4. Results and Discussion

The antenna structure was modeled and simulated using Ansys HFSS. The antenna structure

was excited by using a 50-ohm lumped port and surrounded by an air box with radiation boundaries to simulate open-space conditions. The solution frequency was set at 9 GHz with a linear sweep from 8 to 11 GHz. Adaptive meshing was applied with a maximum of 15 passes and a convergence criterion of 0.02. The reflection, impedance, and far-field radiation were extracted to evaluate resonance behavior, impedance matching, and radiation characteristics.

4.1 Characteristics of Baseline Antenna

The radiation characteristics of the metasurface antennas at 9 GHz are shown in Figure 3. The radiation pattern illustrates how the system directs energy into space and provides insights into its directional capabilities. Figure 3a presents the radiation pattern, where the main lobe is directed broadside, indicating that the metasurface antenna is designed to radiate energy primarily in this direction. The minimal side lobes and back lobes suggest that the system effectively suppresses unwanted radiation in other directions, enhancing efficiency and reducing interference. This configuration serves as a reference, potentially before any modifications are made to improve performance. The perspective of these responses effectively demonstrates the key parameters needed to evaluate the efficiency and performance of a metasurface-based antenna at 9 GHz.

Figure 3b shows the linear gain distribution, highlighting the fundamental beam characteristics before phase variations are introduced through the metasurface design. The y-axis (Phi, φ) represents the horizontal direction, ranging from -180° to 180°, offering insight into how the antenna radiation is distributed in the x-y plane. Similarly, the x-axis (Theta, θ) represents the elevation angle, spanning -180° to 180°, allowing for an analysis of the vertical direction. The peak of a linear gain in this figure reaches approximately 3.63 (5.57 dBi), with the highest concentration of radiation occurring near θ ≈ 0°, indicating a strong broadside-directed beam.

The beam structure in the baseline case is primarily symmetrical and aligned along the broadside direction, indicating that the chessboard-coding metasurface, in its initial configuration, generates a highly focused main beam with minimal deflection. This structured broadside radiation pattern demonstrates the metasurface's ability to effectively manipulate EM waves, producing a well-defined directional beam. The baseline radiation pattern serves as a reference for evaluating the effects of binary defects on beam steering, acting as a benchmark case. When unit-cell defects are introduced, the modifications to the chessboard metasurface resulting from changes in binary coding sequences create anomalous distributions. These alterations can be assessed in relation to the baseline to determine their impact on radiation characteristics.

To investigate impedance behavior, a parametric study was carried out by varying the patch length (L) and aperture width (Ws) of the metasurface antenna, as shown in Figure 4. The antenna is designed to operate at 9 GHz under a series resonance condition introduced by the short-ended feed. Varying L with fixed Ws (1 mm) allowed tuning of the reflection phase for each unit cell. Since AMC performance is highly sensitive to patch dimensions, this tuning ensured consistent phase behavior and preserved the target resonance frequency. Conversely, adjusting Ws with fixed L (3.7 mm) helped reduce mutual coupling between the aperture and metasurface, improving impedance matching.

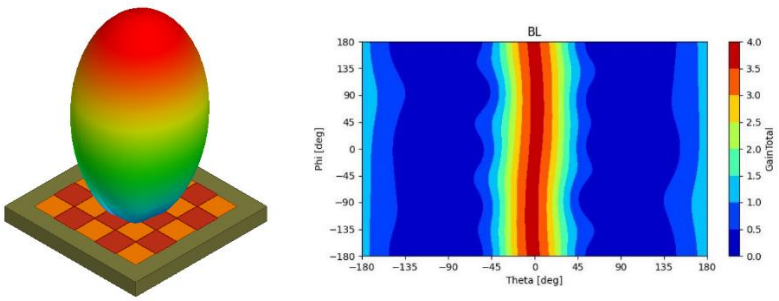

Figure 3 Baseline radiation characteristics of the chessboard-coding metasurface antenna at 9 GHz, (a) illustrating the perspective radiation pattern and (b) showing the gain distribution as functions of the elevation angle (θ) and azimuth angle (φ), centered at θ = 0°, indicating broadside radiation

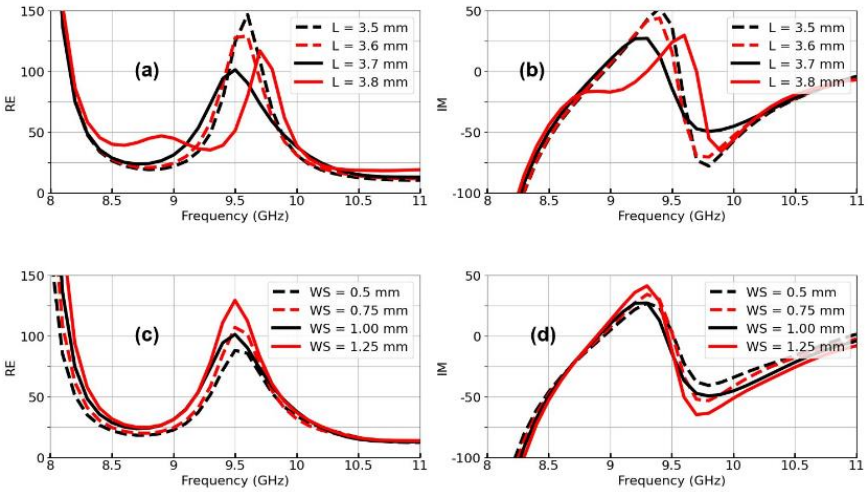

Figure 4 Impedance variations at 9 GHz showing real (Re) and imaginary (Im) components: (a–b) for patch lengths L = 3.5–3.8 mm (fixed Ws = 1 mm), and (c–d) for aperture widths Ws = 0.5–1.25 mm (fixed L = 3.7 mm)

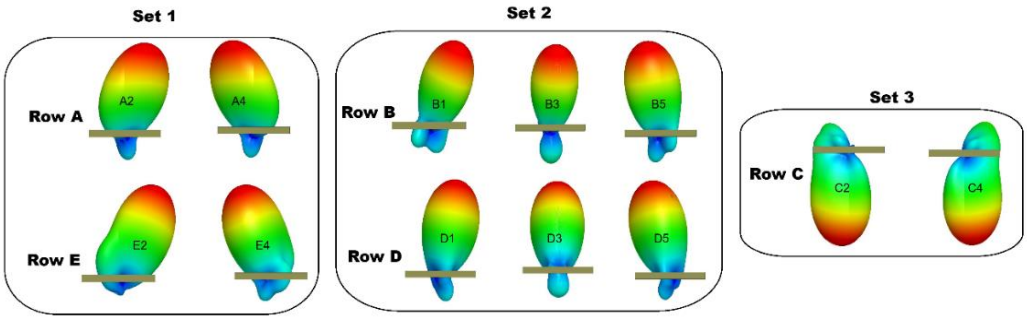

Figure 5 Responses of radiation patterns (a linear gain) in a y-z plane of twelve defective unit cells in a chessboard coding metasurface design, labeled A2, A4, B1, B3, B5, C2, C4, D1, D3, D5, E2, and E4

4.2 Radiation with Binary Defects

Figure 5 presents twelve radiation patterns in linear gain at 9 GHz for the chessboard coding metasurface design with defective unit cells, offering a key visualization of how coding irregularities influence beam shape, direction in the y-z plane (corresponding to the elevation angle θ), and scattering characteristics. Each radiation pattern corresponds to a specific defective unit cell, labeled A2, A4, B1, B3, B5, C2, C4, D1, D3, D5, E2, and E4. These patterns can be categorized into three regional sets based on spatial distribution of defects, determined by the unit cell position within the chessboard pattern. Set 1 (peripheral outer unit cells) includes A2, A4, E2, and E4; Set 2 (centrally located inner unit cells) includes B1, B3, B5, D1, D3, and D5; and Set 3 (side-adjacent inner unit cells) consists of C2 and C4. The variation in these radiation patterns highlights the impact of phase discontinuities and coding defects on the metasurface's ability to manipulate electromagnetic waves. The main radiation lobe provides crucial insights into the efficiency and directivity of beam shaping, which is essential for beam steering applications.

The investigation of Row A (A2 and A4) and Row E (E2 and E4), located at the outer regions of the chessboard pattern, reveals that unit cells maintain a noticeably tilted main lobe. This indicates that defects in these unit cells impact beam distortion at corresponding elevation angles. The beam remains symmetrically upright off-boresight along the y-direction, with variations in direction and shape. A small back lobe is observed in both A2 and A4, though it remains within an acceptable range. These radiation patterns show that while the coding defects influence local phase shifts, the metasurface still provides effective beam control, making it suitable for beamforming with minimal interference.

Next, Set 2, consisting of Row B and Row D, includes unit cells B1, B3, B5, D1, D3, and D5, located at a closer distance compared to Set 1. The evaluation exhibits noticeable beam tilting, but at smaller angles than in Set 1. This suggests that the defective coding sequences in these unit cells introduce symmetry in the wavefronts along the y-direction, except for B3, which remains aligned with the azimuth ($\varphi \approx 0°$). The main lobes of B1, B5, D1, and D5 are slightly displaced from the vertical axis, leading to beam misalignment. Additionally, the presence of low sidelobes indicates that defective unit cells cause non-uniform phase accumulation, resulting in increased energy dispersion in undesired directions.

In Set 3, which includes unit cells C2 and C4 with defects, the radiation patterns exhibit strong asymmetry and increased back-lobe radiation (approximately $\theta \approx 180°$), indicating a significant impact of coding defects on beam performance. The main lobes are no longer well-aligned, and sidelobes become more pronounced. This behavior can be advantageous in applications requiring efficient backward radiation, such as advanced communication networks. The presence of strong back lobes suggests that a portion of the radiated energy is redirected in the opposite direction of the metasurface. These patterns emphasize the critical impact of localized phase discontinuities, demonstrating that even minor defects in unit-cell coding can significantly alter global radiation characteristics.

To observe the effect in the azimuth direction, Figure 6 presents the top-view radiation patterns (x-y plane) for ten defective unit cells (excluding C2 and C4, which exhibit backward re-direction) in a chessboard coding metasurface design. The unit cells are categorized into small groups based on their spatial distribution of defects within the array and associated phase discontinuities. The presence of defective unit cells alters the expected beam directionality, affecting the wave manipulation efficiency. The radiation patterns are classified into three groups: Group 1 (A2, A4, E2, and E4), Group 2 (B1, B5, D1, and D5), and Group 3 (B3 and D3). All radiation patterns maintain a strong main lobe in an off-boresight direction.

Group 1 exhibits significant beam tilting and highly symmetric radiation patterns, with main lobes deviating sharply from the broadside direction along the x and y-axis. The E2 and E4 unit cells display greater beam tilting than A2 and A4, indicating that defects in these unit cells cause substantial phase disruptions, impairing the metasurface ability to maintain a controlled and focused beam.

Group 2 demonstrates moderate beam tilting while maintaining a more structured main lobe compared to Group 1. The symmetric unit cells B1, B5, D1, and D5 show radiation patterns along the x and y-axis indicative of spatial diffraction effects due to phase inconsistencies. This group represents a transitional phase, where defective coding influences wavefront control, but beam distortion remains manageable. Group 3 exhibits stable and symmetric radiation patterns along only the x-axis, maintaining well-centered main lobes with minimal phase disturbance from coding defects. The beam directions remain close to the broadside, suggesting that these unit cells retain better phase integrity compared to those in the previous groups.

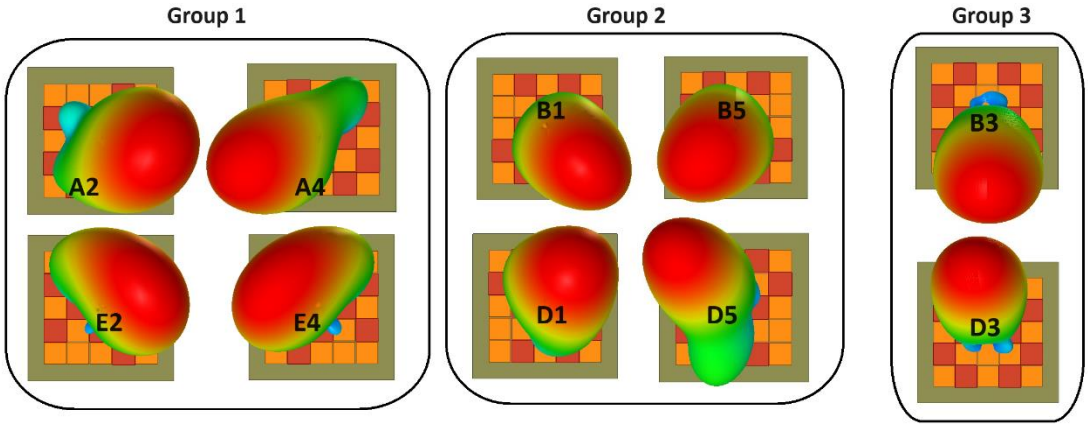

Figure 6 Top-view radiation patterns (a linear gain) in a z-y plane of ten defective unit cells in a chessboard coding metasurface design

The twelve radiation patterns reveal the varying impact of coding defects in a chessboard-coding metasurface. While some defective unit cells cause beam distortion, others result in significant misalignment, pronounced sidelobes, and increased energy scattering. These findings are essential for understanding the practical challenges of implementing metasurface designs in real-world applications. In beamforming and wireless communication, coding defects can degrade signal strength and increase interference, negatively affecting overall system performance. Addressing these defects is crucial for enhancing directivity and ensuring efficient radiation control in advanced metasurface-based technologies.

4.3 Effect of Binary Defects on Reflection

Reflection (S_{11}) responses are essential for evaluating the performance of a chessboard-coding metasurface antenna. This parameter provides critical insights into the matching properties, which are essential for optimizing metasurface antenna design.

The reflection coefficient is plotted as a function of frequency, measured in dB. Figure 7 illustrates the reflection coefficient characteristics for twelve unit-cell configurations with defects in a chessboard coding metasurface design. A low reflection coefficient (S_{11} less than −10 dB) is desirable, with a pronounced dip around 9 GHz in the baseline. Each subplot corresponds to a specific defective unit cell, labeled A2, A4, E2, E4, B1, B5, D1, D5, B3, D3, C2, and C4. The primary objective of this analysis is to investigate how binary coding defects influence the resonant frequency, depth of reflection nulls, and operational bandwidth. In an ideal chessboard-coding metasurface, the reflection follows a predictable resonance due to its periodic binary phase coding (0° and 180°), which facilitates controlled scattering and reflection. However, defects in the binary sequence disrupt the phase balance, leading to resonance shifts, multiple reflection dips, and variations in reflection depth.

Most unit cells show stable resonance with minimal distortion, except for C2 and C4, which display a noticeable shift in the reflection dip. These unit cells exhibit multiple dips in the reflection coefficient, indicating the presence of additional resonance modes despite coding defects. The deep reflection dips suggest good impedance matching and efficient wave absorption around 9 GHz, except for A4, which shows increased reflection, indicating poorer impedance matching. This phenomenon, known as resonance splitting, occurs when localized phase discontinuities introduce unwanted scattering, leading to secondary resonances. The wider bandwidth resulting from these secondary resonances may be beneficial for applications requiring broadband metasurface functionality. However, the slight distortions in the reflection curve imply that the defects cause minor phase perturbations, slightly broadening the resonance bandwidth and affecting phase uniformity.

Defective cells C2 and C4 exhibit weak resonance and degraded reflection performance. In these unit cells, the reflection coefficient does not drop significantly below −10 dB, indicating poor impedance matching and higher reflection losses. These coding defects likely introduce mutual impedance effects, disrupting the expected resonance. The phase mismatches across these unit cells result in partial destructive interference instead of complete cancellation at the resonance frequency.

Figure 8 shows the reflection phase responses of twelve unit cells from a chessboard-coding metasurface antenna, compared to a baseline (non-defective) antenna. The baseline exhibits a sharp phase shift near 9 GHz, indicating normal resonance behavior. In contrast, the defective cells show varying deviations, including shifted resonance points and uneven phase transitions. These differences are most noticeable in the 8.5–9.5 GHz range, which is important for beam steering. The results show that binary defects disrupt the phase profile, leading to beam tilting and distortion. The impact also depends on the location of the defect in the metasurface, supporting a classification into inner and outer regions. This highlights the importance of spatial placement in designing metasurfaces that can tolerate defects.

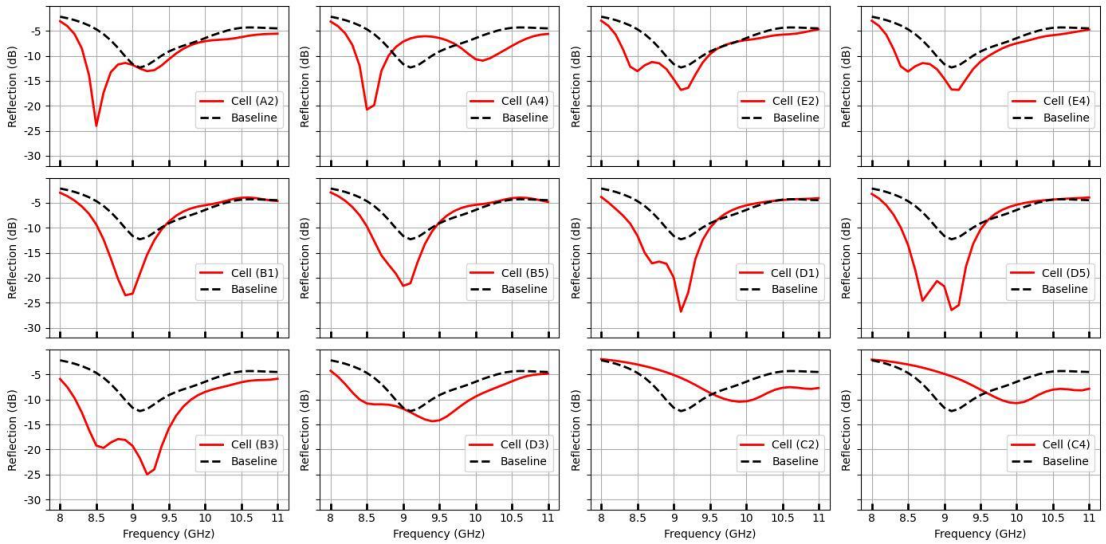

Figure 7 Characteristics of reflection coefficients of twelve defective unit cells (A2, A4, E2, E4, B1, B5, D1, D5, B3, D3, C2, and C4), compared to the baseline and plotted as a function of frequency (8–11 GHz)

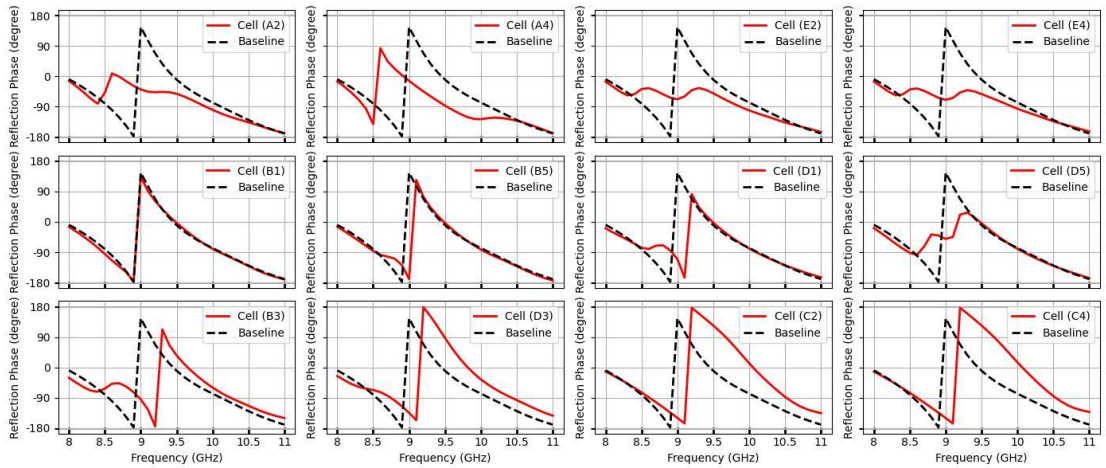

Figure 8 Reflection-phase responses of twelve defected unit cells, consisting of A2, A4, E2, E4, B1, B5, D1, D5, B3, D3, C2, and C4, compared to the baseline and plotted as a function of frequency (8–11 GHz)

4.4 Effect of Binary Defects on Impedance

The real part of the impedance represents the resistive component of the antenna impedance. In practical antenna designs, an impedance close to 50 ohms is preferred to ensure maximum power transfer. The real impedance plot indicates that, at 9 GHz, the impedance value is relatively stable and close to 50 ohms. To analyze the impedance behavior, the real part of the impedance for twelve defective unit-cell configurations in a chessboard coding metasurface design is plotted as a function of frequency over the 8–11 GHz range. Figure 9 illustrates the real part of the impedance (Re), with each subplot corresponding to a specific defective unit cell, labeled A2, A4, E2, E4, B1, B5, D1, D5, B3, D3, C2, and C4. However, binary coding defects introduce phase discontinuities that significantly affect the impedance behavior, leading to resonance shifts and multiple peaks. The analysis of real impedance variations across these unit cells reveals distinct impedance characteristics and their influence on metasurface performance.

All defective cases, except for the C2 and C4 unit cells, exhibit a smooth decrease in real impedance with frequency and show double-tuned impedance matching near 9 GHz. This gradual variation indicates a stable frequency response, making these cells suitable for wideband metasurface designs that

require low distortion and consistent wave control. However, the presence of multiple resonance peaks and sharp impedance shifts at certain frequencies suggests resonance splitting caused by binary coding defects. These effects are likely due to mode coupling, which can lead to energy loss at unintended frequencies. The variation in real impedance among unit cells plays a critical role in overall metasurface performance. In contrast, cells such as C2 and C4, which show poor resistance matching around 9 GHz, demonstrate degraded resonance behavior and are more prone to performance instability.

The imaginary part of the impedance represents the reactive component of the antenna. Figure 10 presents the responses of the imaginary part (Im) for twelve defective unit-cell configurations in a chessboard coding metasurface, plotted as a function of frequency (GHz). At resonance, the imaginary part should approach zero to minimize reactive power losses and maximize power transfer efficiency. The imaginary impedance is near zero at 9 GHz, confirming that the system operates efficiently at this frequency with minimal reactive losses. All defective unit cells, except C2 and C4, exhibit multiple reactance conditions and resonance splitting. These unit cells display significant fluctuations in their imaginary impedance, characterized by multiple zero-crossing points. The presence of multiple reactance peaks indicates resonance splitting, caused by phase discontinuities introduced by coding defects. In contrast, C2 and C4 show minimal influence near the zero-crossing points, indicating reduced resonance.

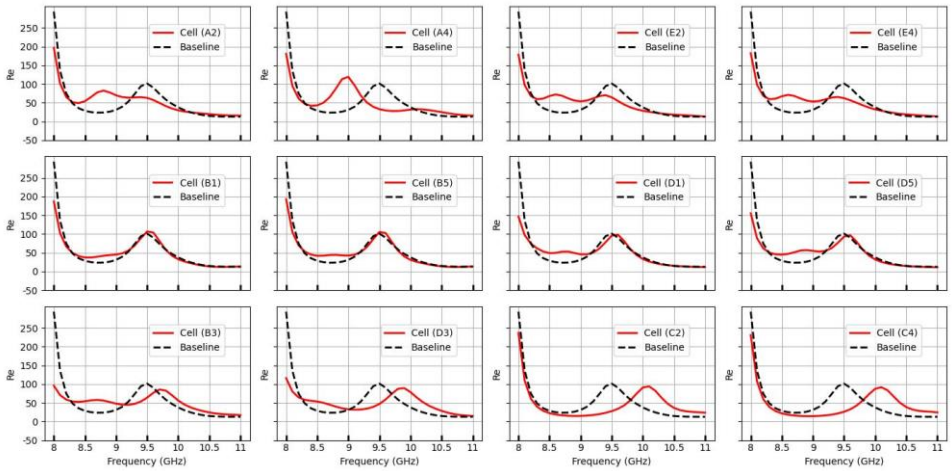

Figure 9 Real part responses (Re) of impedance (compared to the baseline) for twelve defective unit cells, consisting of A2, A4, E2, E4, B1, B5, D1, D5, B3, D3, C2, and C4, plotted as a function of frequency (8–11GHz)

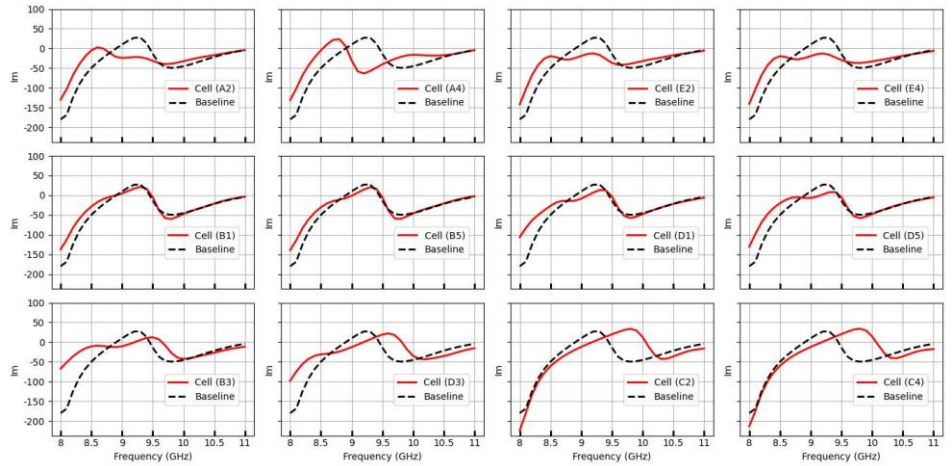

Figure 10 Imaginary-part responses (Im) of impedance (compared to the baseline) for twelve defective unit cells, consisting of A2, A4, E2, E4, B1, B5, D1, D5, B3, D3, C2, and C4, plotted as a function of frequency (8–11 GHz)

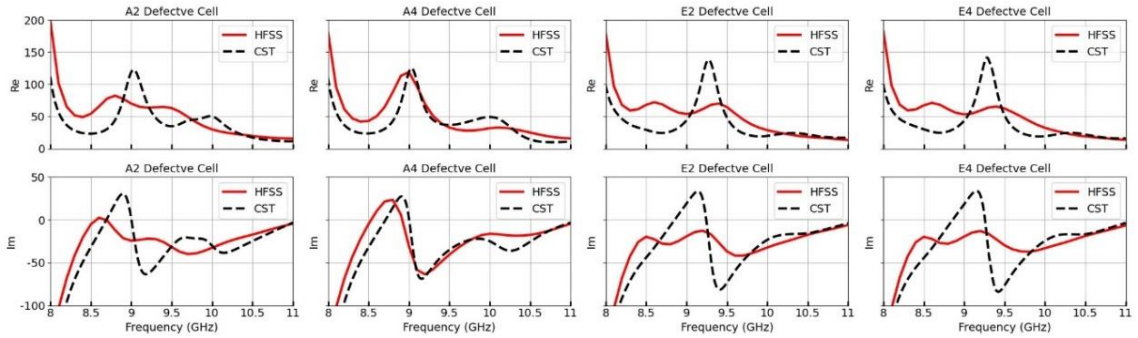

Figure 11 Comparison of real (Re) and imaginary (Im) impedance components for four defective unit cells (A2, A4, E2, and E4), simulated using Ansys HFSS and CST Studio Suite

To validate the simulated impedance characteristics, CST Studio Suite (Dassault Systèmes., 2024) was used alongside the Ansys HFSS solver for cross-verification. Figure 11 presents a comparative analysis of the impact of binary defects on antenna impedance, focusing on four representative cases: A2, A4, E2, and E4. These cases correspond to different spatial positions of defects within the metasurface, enabling evaluation of their localized influence on impedance behavior. Full-wave simulations from both Ansys HFSS and CST Studio Suite show comparable behavior, confirming that the position of binary defects significantly affect both the resistive and reactive components of the antenna impedance. The minor variations between Ansys HFSS and CST Studio Suite simulations are attributed to differences in the port excitation models used to excite the feed structure.

4.5 Characteristics of Gain Distribution

The gain distribution illustrates the beam characteristics and directivity, emphasizing the impact of unit-cell defects in the metasurface antennas (A2, A4, E2, E4, B1, B5, D1, D5, B3, D3, C2, and C4), which are crucial for beamforming, radiation control, and electromagnetic wave manipulation, as shown in Figure 12. These gain characteristics (linear gains) demonstrate how binary coding metasurface defects affect wave reflection and beam symmetry. In particular, they highlight the influence of radiation caused by the unit cells with out-of-phase change in the targeted coordinate system within the chessboard pattern. The beam-tilting effect is presented through a comparative analysis of the radiation behavior, where modifications in the binary coding sequence alter the unit cells. In the far-field gain patterns, the maximum gain varies from approximately 2.5 (3.9 dBi) to 3.3 (5.3 dBi) for all defected unit cells, except for C2 and C4, which exhibit a decreased peak gain of approximately 2.0 (3.1 dBi). This indicated the metasurface's efficiency in directing radiated energy toward specific angular regions. These gains result in a slight drop compared to the baseline value of 3.63 (5.57 dBi).

When analyzing the θ (elevation) and φ (azimuth) angles, the modified unit cells cause a shift in the main beam, resulting in the beam tilting toward off-boresight angles. This causes the beam to shift away from the broadside and tilt toward both the right and left when the A2, A4, B1, and B5 cells are defected. Symmetric high-gain regions appear in azimuth (φ) at approximately ±100° for A2 and A4, ±50° for B1 and B5, and in elevation (θ) at +25° for A2 and A4, and +17.5° for B1 and B5. These results confirm that changes in the binary coding sequence effectively redistribute energy within the metasurface. This enables adaptive beam tilting with step sizes of $\Delta\theta = 7.5°$ (elevation) and $\Delta\varphi = \pm 50°$ (azimuth).

In regions where the beam tilts at similar elevation angles of +17.5° for D1, D5, E2, and E4, prominent high-gain regions are observed at approximately ±137° for D1 and D5, ±110° for E2 and E4 in azimuth (φ). These findings further support the ability of modifications to the binary coding sequence to facilitate dynamic energy redistribution. Facilitates adaptive beam steering with no change in elevation and $\Delta\varphi = \pm 27°$ in azimuth.

For tilt only in the up and down directions, the phase modifications at B3 and D3 cause a shift in the main beam, resulting in radiation patterns along the x-direction. Notable high-gain regions emerge at approximately +22.5° in elevation (θ) and at +0° and −10° in azimuth (φ), indicating wavefront distortions due to phase mismatches. These results confirm that modifying the binary coding sequence enables dynamic energy redistribution within the metasurface, enhancing adaptive beam tilting performance along the ±x direction.

Specifically, the phase modifications at C2 and C4 cause a deviation in the main beam direction, resulting in a backward radiation pattern. Distinct high-gain regions appear at approximately +180° in elevation (θ), indicating wavefront distortions caused by out-of-phase mismatches. These findings confirm that altering the binary coding sequence facilitates dynamic energy redistribution in the reverse direction relative to broadside.

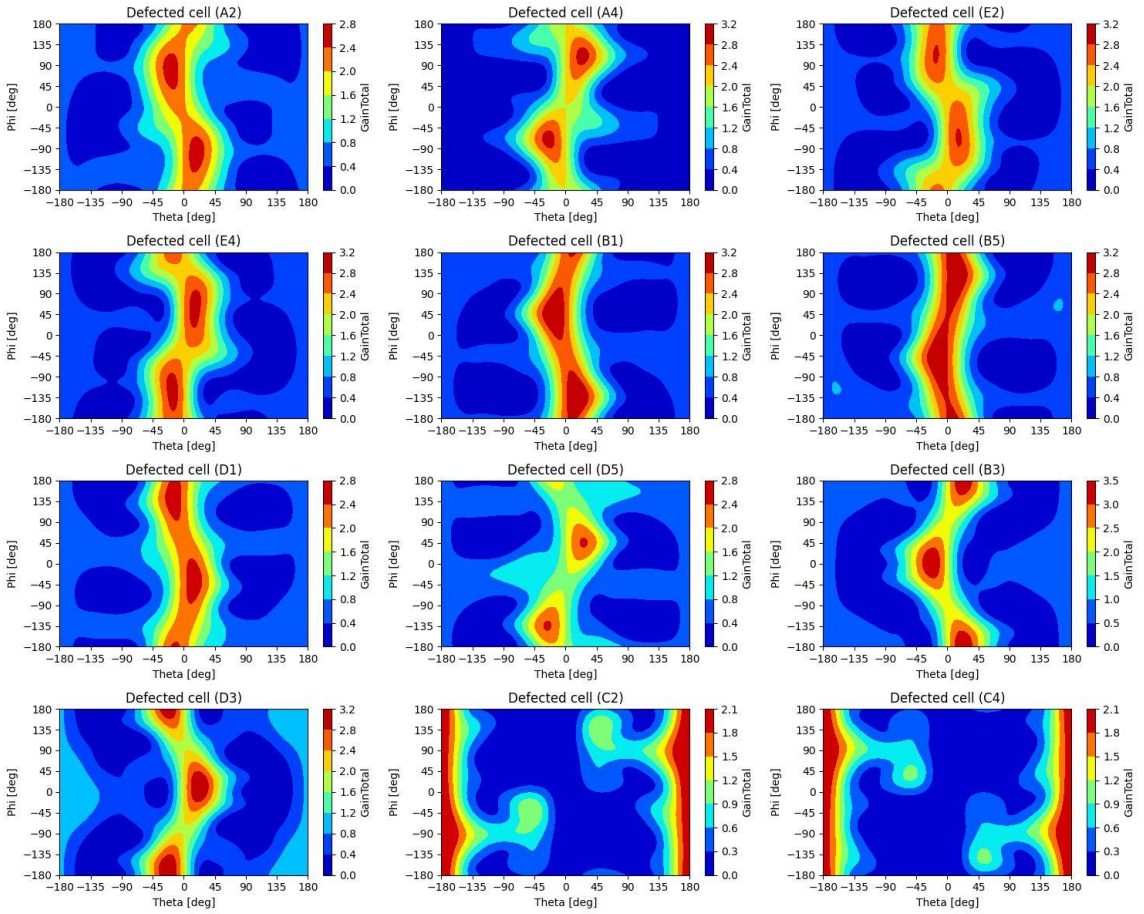

Figure 12 Gain distribution (linear gains) comparison of the chessboard-coding metasurface antenna with the defected unit cells, consisting of A2, A4, E2, E4, B1, B5, D1, D5, B3, D3, C2, and C4

Table 2 Beam-tilted direction and gain for different defective metasurface unit cells in terms of Theta (θ) and Phi (φ) angles in degrees. The table presents the beam direction for each unit cell, including A2, A4, E2, E4, B1, B5, D1, D2, B3, D5, C2, and C4. (Baseline θ ≈ 0°)

Defected Cell	**A2**	**A4**	**E2**	**E4**
θ (elevation)	+25°	+25°	+17.5°	+17.5°
φ (azimuth)	+100°	−112.5°	+110°	−115°
Gain (dBi) with a linear value	4.39 dBi (2.75)	4.67 dBi (2.93)	4.52 dBi (2.83)	4.68 dBi (2.94)
Defected Cell	**B1**	**B5**	**D1**	**D5**
θ (elevation)	+17.5°	+17.5°	+17.5°	+17.5°
φ (azimuth)	+50°	−50°	+137°	−137°
Gain (dBi) with a linear value	5.04 dBi (3.19)	4.98 dBi (3.16)	4.12 dBi (2.58)	4.05 dBi (2.54)
Defected Cell	**B3**	**D3**	**C2**	**C4**
θ (elevation)	+22.5°	+22.5°	+175°	+175°
φ (azimuth)	0°	−10°	–	–
Gain (dBi) with a linear value	5.25 dBi (3.35)	5.01 dBi (3.17)	3.18 dBi (2.08)	3.12 dBi (2.05)

Table 2 summarizes the angles (in degrees) of a radiation beam direction and gain-peak (in dBi) responses for individual different defective metasurface unit cells in terms of Theta (θ) elevation and Phi (φ) azimuth angles. It compares unit cells A2, A4, E2, E4, B1, B5, D1, D2, B3, D5, C2, and C4, showing their respective beam directions relative to the baseline ($\theta \approx 0°$). The values highlight significant deviations, indicating notable changes in beam steering behavior. The results demonstrate how modifications in specific unit cells influence radiation direction, with elevation and azimuth angles tilting almost symmetrically, highlighting the adaptability for beamforming applications.

4.6 Implications and Future Work

This study presents the concept of a defect-aware chessboard-coded metasurface integrated into a planar antenna, where the spatial impact of binary defects is not merely analyzed, but intentionally leveraged as a design parameter. By recognizing that localized defects within the periodic coding pattern can systematically influence beam direction, gain, and impedance, designers are empowered to either compensate for or harness these effects to improve overall antenna performance. A key implication is that such defect-aware metasurface designs enable precise manipulation of radiation wavefronts, supporting dynamic beam tilting in both elevation and azimuth enhancing adaptability for advanced 6G wireless communication systems in the centimeter-wave band.

Building on the current simulation insights, future research will focus on several key directions. First, performance improvements related to gain enhancement and structural configurations that support greater beam tilting under increased defect conditions will be investigated. Experimental validation through the fabrication and measurement of prototype metasurface antennas is essential to confirm the effects of binary defects on beam direction and gain. Additionally, integrating tunable components such as PIN diodes or varactors will enable real-time control of defect states, supporting dynamic beam reconfiguration. Another important focus is the modeling of clustered or irregular defect patterns, which will help establish robust design strategies for large-aperture, defect-resilient metasurfaces. Furthermore, the application of machine learning techniques, such as data-driven optimization, could assist in predicting optimal defect configurations and compensation strategies, enhancing adaptive performance in practical scenarios.

5. Conclusion

This research presents a numerical investigation of digital chessboard-coding metasurface antennas utilizing binary defects for beamforming applications. The proposed 1-bit phase-coded metasurface demonstrates significant advancements in beam reconfiguration by leveraging a binary ‘0’ and ‘1’ phase coding strategy. The results indicate that binary defects effectively enhance beam control, enabling radiation pattern reconfiguration. Full-wave FEM simulations show that binary-defected metasurfaces can modulate beam direction in both azimuth and elevation.

A total of the twelve defective unit cell configurations within a 5 × 5 lattice were analyzed, revealing four distinct spatial response behaviors. Defects positioned at the corners of the outer lattice provide an elevation angle of approximately +17.5° and +25° with azimuth angles of ±110°, while inner lattice corner defects provide similar elevation angles with azimuth angles around ±50° and ±137°. Central defects along the electric field give an elevation of +17.5° with azimuth angles of +2.5° and +177.5°, while those along the magnetic field give similar elevation angles both of +180°, resulting in the radiation of the backward redirection. The antenna gains peaks range from 4.1 to 5.3 dBi for defective configurations, except for backward radiation at 3.1 dBi, with a baseline gain of 5.57 dBi. The impedance bandwidths are approximately observed within the 8.4–9.5 GHz frequency range.

While the simulation results are promising, experimental validation is essential to confirm the real-world performance of binary-defected metasurface antennas. The findings contribute to the growing field of reconfigurable intelligent surfaces and pave the way for future advancements in metasurface antenna technology.

6. Acknowledgements

The authors would like to thank the College of Computing, Prince of Songkla University, Phuket Campus, Thailand, for their support.

7. CRediT Statement

Tanatorn Tantipiriyakul: Conceptualization; Software; Methodology; Writing – original draft; Investigation; Formal analysis; Visualization.

Komsan Kanjanasit: Conceptualization; Methodology; Software; Writing – original draft; Investigation; Formal analysis; Visualization; Writing – review & editing; Supervision.

8. References

Ansys Inc. (2024). *Ansys HFSS – Student Version* [Computer software]. Ansys Inc. Retrieved from https://www.ansys.com/academic/students

Balanis, C. A. (2005). *Babinet's principle. In Antenna Theory: Analysis and Design* (3rd ed.). Hoboken, NJ: John Wiley & Sons.

Cui, T. J., Li, L., Liu, S., Ma, Q., Zhang, L., Wan, X., ... & Cheng, Q. (2020). Information metamaterial systems. *Iscience*, *23*(8), Article 101403. https://doi.org/10.1016/j.isci.2020.101403

Cui, T. J., Liu, S., & Li, L. L. (2016). Information entropy of coding metasurface. *Light: Science & Applications*, *5*(11), Article e16172. https://doi.org/10.1038/lsa.2016.172

Cui, T. J., Qi, M. Q., Wan, X., Zhao, J., & Cheng, Q. (2014). Coding metamaterials, digital metamaterials and programmable metamaterials. *Light: Science & Applications*, *3*(10), Article e218. https://doi.org/10.1038/lsa.2014.99

Dassault Systèmes. (2024). *CST Studio Suite – Student Edition* [Computer software]. Dassault Systèmes. Retrieved from https://www.3ds.com/edu/education/students/solutions/cst-le

Feresidis, A. P., Goussetis, G., Wang, S., & Vardaxoglou, J. C. (2005). Artificial magnetic conductor surfaces and their application to low-profile high-gain planar antennas. *IEEE Transactions on Antennas and Propagation*, *53*(1), 209-215. https://doi.org/10.1109/TAP.2004.840528

Galarregui, J. C. I., Pereda, A. T., De Falcon, J. L. M., Ederra, I., Gonzalo, R., & De Maagt, P. (2013). Broadband radar cross-section reduction using AMC technology. *IEEE Transactions on Antennas and Propagation*, *61*(12), 6136-6143. https://doi.org/10.1109/TAP.2013.2282915

Kanjanasit, K., Osklang, P., Jariyanorawiss, T., Boonpoonga, A., & Phongcharoenpanich, C. (2023). Artificial magnetic conductor as planar antenna for 5G evolution. *Computers, Materials & Continua*, *74*(1). 503–522. https://doi.org/10.32604/cmc.2023.032427

Ma, Q., Xiao, Q., Hong, Q. R., Gao, X., Galdi, V., & Cui, T. J. (2022). Digital coding metasurfaces: From theory to applications. *IEEE Antennas and Propagation Magazine*, *64*(4), 96-109. https://doi.org/10.1109/MAP.2022.3169397

Rahman, M. M., Yang, Y., & Dey, S. (2025). Application of metamaterials in antennas for gain improvement: A study on integration techniques and performance. *IEEE Access*, *13*, 49489 – 49503. https://doi.org/10.1109/ACCESS.2025.3552023

Selvaraj, M., Vijay, R., & Anbazhagan, R. (2025). Reflective metasurface for 5G & beyond wireless communications. *Scientific Reports*, *15*(1), Article 126. https://doi.org/10.1038/s41598-024-84523-9

Sheng, L. L., Cao, W. P., Mei, L. R., & Yu, X. H. (2022). A novel low-cost beam-controlling antenna based on digital coding metasurface. *International Journal of RF and Microwave Computer-Aided Engineering*, *32*(6), Article e23152. https://doi.org/10.1002/mmce.23152

Simons, R. N. (2001). Coplanar waveguide short circuit. *In Coplanar Waveguide Circuits, Components, and Systems.* (1st Ed). New York, NY: Wiley-Interscience.

Tantipiriyakul, T., & Kanjanasit, K. (2023). Design and simulation of chessboard coding wave artifacts. *Journal of Information Science and Technology*, *13*(2), 62-68. https://doi.org/10.14456/jist.2023.13

Tantipiriyakul, T., & Kanjanasit, K. (2024). A Binary Hexagon Stripe Metamaterial Antenna [Conference presentation]. *2024 21st International Conference on Electrical Engineering/Electronics, Computer, Telecommunications and Information Technology (ECTI-CON)*. IEEE, Khon Kaen, Thailand. https://doi.org/10.1109/ECTI-CON60892.2024.10594859

Testolina, P., Polese, M., & Melodia, T. (2024). Sharing spectrum and services in the 7–24 ghz upper midband. *IEEE Communications Magazine*, *62*(8), 170-177. https://doi.org/10.1109/MCOM.001.2400086

Vinod, G. V., & Khairnar, V. V. (2024). A wideband beam steering and beamwidth reconfigurable antenna using coding metasurface. *IEEE Access*, *12*, 97143–97153. https://doi.org/10.1109/ACCESS.2024.3427707

Wang, S., Xu, H. X., Wang, M., & Tang, S. (2024). A low-RCS, high-gain and polarization-insensitive FP antenna combing frequency selective rasorber and metasurface. *IEEE Open Journal of Antennas and Propagation*, *5*(6), 1623–1628. https://doi.org/10.1109/OJAP.2024.3426624

Xue, J., Jiang, W., & Gong, S. (2017). Chessboard AMC surface based on quasi-fractal structure for wideband RCS reduction. *IEEE Antennas and Wireless Propagation Letters*, *17*(2), 201-204. https://doi.org/10.1109/LAWP.2017.2780085

Zhang, L., & Cui, T. J. (2021). Space-time-coding digital metasurfaces: Principles and applications. *Research*. 2021, Article 9802673. https://doi.org/10.34133/2021/9802673

Zhang, L., Wan, X., Liu, S., Yin, J. Y., Zhang, Q., Wu, H. T., & Cui, T. J. (2017). Realization of low scattering for a high-gain Fabry–Perot antenna using coding metasurface. *IEEE Transactions on Antennas and Propagation*, *65*(7), 3374-3383. https://doi.org/10.1109/TAP.2017.2700874